ORIGINAL ARTICLE

Depicting the main structural affected trends by operating aeromagnetic survey in the western part of Koraimat-Alzafarana road and surround area, Eastern Desert, Egypt

Alaa M. Eweis[1] · **Mostafa Toni**[1] · **Alhussein Adham Basheer**[1]

Abstract

Aeromagnetic data of the western part of Koraimat-Alzafarana road, Eastern Desert, Egypt is interpreted to detect the subsurface structures that may resulted in presence of subsurface aquifer. To reach to the main target of this study, many procedures are done using some magnetic analysis techniques (e.g., technique of reduction to the magnetic pole, separation technique of regional-residual anomalies and edge detection methods). The results have been encouraging to merit further estimation of the magnetic depth and analyzing the trends of the study area. To increase the credibility, the depth is revised by the P-depth technique. The shallow and deep magnetic components are calculated to be 2046 and 5680 m. To ease the detection of the structure that encasing the study area and lack the rigorous analysis, reduced the magnetic pole map, residual map and 3D Euler deconvolution are integrated to depict the combined lineament map that prevailing tectonic pattern of the study area. Eventually, NE–SW trend is the predominant structural trend affecting on the study area as deducing from magnetic anomalies. Moreover, there are minor structural trends which were taken N–S, NW–SE, W–E, NNW–SSE and NNE–SSW directions. The presence of subsurface structures may assist in the occurrence and recharging of the groundwater aquifers.

Keywords Aeromagnetic data · Interpretation techniques · Koraimat-Alzafarana road and surrounding area in Egypt · Subsurface structures

Introduction

The Egyptian government tends to plan new urban communities capable of accommodating industrial development and increasing population growth. The western part of Koraimat-Alzafarana road and surrounding area is one of the new promising areas which is approved for the establishment of a new projects and buildings (MHUUD 2015). The area is very important to be used in any sustainable development project which locate near to the Nile River (MHUUD 2015). It is necessary to know the subsurface structure of any new investigated area which is recognized as an underground system that may be capture runoff and gradually infiltrate it into the groundwater through rock and gravel (Geosyntec 2004). There are many previous geological and geophysical works that applied by authors Khalil et al. (2016), Saber and Salama (2017), Tahoun et al. (2017), Zahran et al. (2011), Sayed et al. (2021) and Mosaad and Kehew (2019) in the surrounding area of the study area.

Geophysical surveys are used to image and detect the subsurface structures (Exploration Geophysics 2020). It also used in monitoring environmental impact, mapping subsurface archaeological sites, investigations the subsurface ground water, and mapping the subsurface salinity (Exploration Geophysics 2020).

The magnetic method is one of the best and easiest tools to determine the depth of basement according to the variation in magnetic sensitivity due to the difference in mineral compositions and lithology of rocks (Waheed 2019). Basically, the magnetic survey measurements depend on determine the magnetic-field intensity, magnetic inclination, and declination at several stations (Reeves 2005) and (Aero

✉ Alaa M. Eweis
  alaa.magdy@science.helwan.edu.eg

  Mostafa Toni
  mostafa.toni@science.helwan.edu.eg

  Alhussein Adham Basheer
  alhussein.adham@science.helwan.edu.eg

1 Geology Department, Faculty of Science, Helwan University, 11795 Ain Helwan, Cairo, Egypt

Service 1984). The aim of the study is depicting the main subsurface structure using aeromagnetic survey.

Location and geological setting of the study area

The present study area (The western part of Koraimat-Alzafarana road) and its surrounding area locates in the stable shelf of Egypt (Said 1962), on the eastern bank of the Nile River in the Eastern desert of Egypt (Fig. 1a, b). The surface topography of the study area ranges between 50 and 750 m related to the sea level (Lisle 2006); (EROS) (Fig. 1a, b). The area is about 3612.68 Km^2 which covers dominantly by Quaternary and Tertiary deposits. The main geological units that represent the study are shown in Fig. 1c, which are modified from the geological map of Egypt prepared by CONOCO (1987). The study area consists of Limestone of Cretaceous and Tertiary ages and covered by Quaternary deposits. The Cretaceous to Quaternary are incorporated in Mokattam Formation (Fm), Wadi Rayan Fm, Maadi Fm, Beni Suef Fm, Maghara formation and Raqaba Fm (Fig. 1c). These formations are described as follow: Mokattam Group: which consists of observatory Formation shallow marine, dense medium bedded limestone with local chert, Pliocene deposits composed of loose deposits (North of Faiyum possibly younger) (CONOCO 1987), Umm Raqaba Formation: composed of yellow marine fossiliferous sandstone with shale stringers alternating with conglomerates of limestone, chert and quartz pebbles, quaternary deposits: consists mainly of sand dunes, Nile silt, playa deposits, wadi deposits and gravels, Mokattam group wadi Rayan formation: consists of shallow marine limestone repeatedly intercalated by shale and sandy shale, Mokattam group Beni Suef formation: composed of marine shale, marl, and limestone, Oligocene deposits: consists of gravel and sands, Mokattam group Maghagha formation: composed of open marine limestone and marl, in the east underlain by shale, Cretaceous deposits: composed of sequence of chalky limestone, Maadi formation: composed mainly of shallow marine shale and limestone, Thebes Group: composed of Abu Rimth formation that is composed of well-bedded shelf limestone and marl (CONOCO 1987).

Methodology

The Aero-Services company carried out a rapid reconnaissance aeromagnetic survey in 1983 in the western part of Koraimat-Alzafarana road and surrounding area as a part of

Mineral, Petroleum and Groundwater Assessment Program (MPGAP) (Lisle 2006) and (EROS). The airborne survey used a proton free—precision magnetometer (Varian, V-85), with a sensitivity (0.01nT) (Aero Service 1984). The survey is made by gridding over the area and making measurements at each station on the grid to image the subsurface structures which the flight is directed to flight path NE-SW directions and flown along parallel traversed lines with azimuth of 25° and 225° by lines spacing 1.5 km. The flight is flown along tie-lines with azimuth of 135° and 315° and space between the lines equal to 5 km (Aero Service 1984) (Fig. 2a). To increase the accuracy of collecting data during the survey, the controlled time is adjusted to international time using radio with short wave (Aero Service 1984).

The collected data are enhanced and converted to contour lines which match the equal values together to create a magnetic intensity map with a good reflected magnetic anomaly. This magnetic anomaly represented variation between the magnetic field of the earth and the secondary magnetic field (Aero Service 1984). These variations represented in variable rocks that distributed over the crust surface (Sordi 2007). These rocks and minerals which have a strong magnetic susceptibility generate a secondary magnetic field which in turn effect on the magnetic field of the earth (Reford 1962). So, a good aeromagnetic interpretation depends basically on a good identification of geological setting (lithology and stratigraphy) of the study area (Aero Service 1984).

By processing the data collected by aeromagnetic survey and by applying the filters technique like spectral analysis technique (Salem et al. 2000; Nwankwo 2014; Alasi et al. 2017) analytical signal technique (Joshua et al. 2018), Edge detection techniques (Miller and Singh 1994; Verduzco et al. 2004a, b; Silva and Barbosa 2003) and Euler deconvolution techniques (Silva and Barbosa 2003), a good interpretation for the data is predicted to demarcate the subsurface structure of the area under investigation.

Data-analysis and interpretation

The aeromagnetic data are enhanced to delineate the depth of basement in the area under investigation and to infer the tectonic and earth's structure history using the qualitative and quantitative methods. The collected data from the airborne magnetometer are enhanced to display an aeromagnetic map that oriented to the magnetic field with Inclination angle equal to 39° and Declination angle equal to 2°. The aeromagnetic map is digitized using Didger program (Didger 2008). The output is processed as a colored map with intensity ranged between minimum value (41,496 nT)
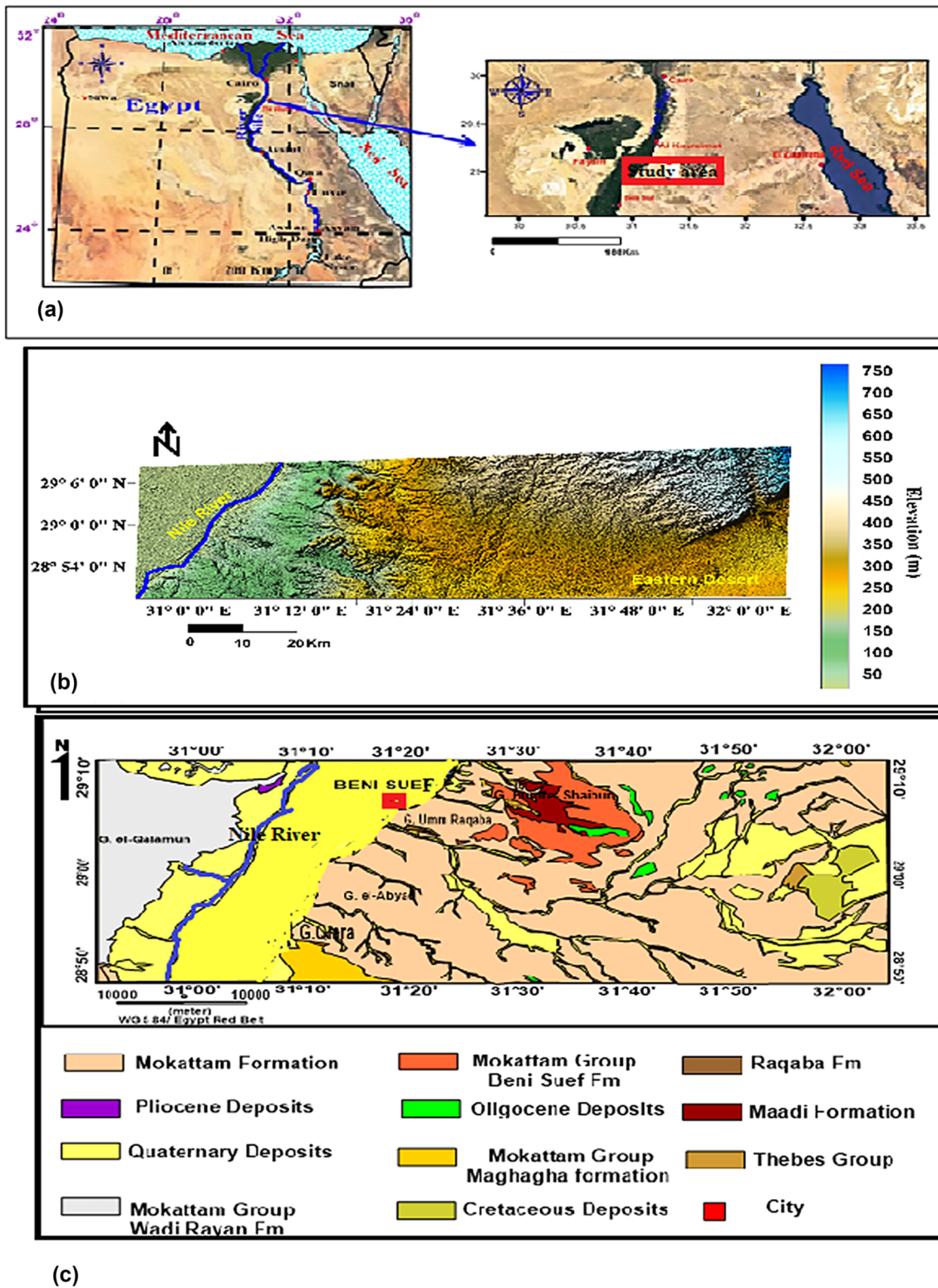
Fig. 1 **a** Map of Egypt showing general location of the study area (Lisle 2006). **b** Topographic map of the study area (EROS). **c** Geologic map of the study area modified after (CONOCO 1987)
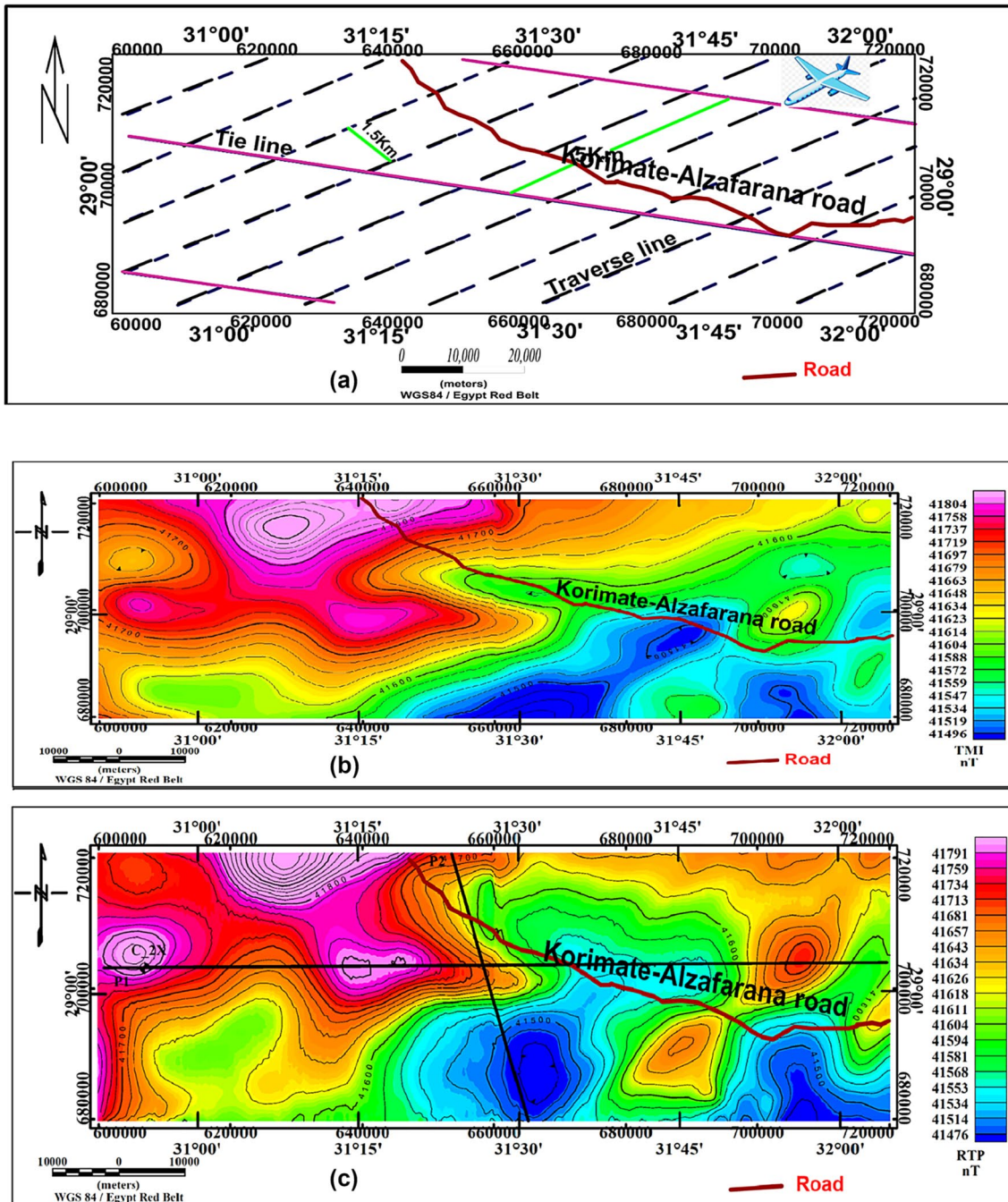
Fig. 2 **a** Flight path of the MPGAP project, specifications modified after (Aero Service 1984). **b** Total aeromagnetic intensity map of the study area. **c** The RTP map derived from the aeromagnetic field intensity map with the location of two profiles along the study area

and maximum value (41,804 nT) that represents a total aeromagnetic intensity (TMI) map (Fig. 2b). The TMI map is

described by high magnetic anomalies (positive amplitude with Red color) and low magnetic anomalies (negative

amplitude with Blue color) in which high anomalies are large distributed in the north and west directions of the study area with a circular closure shapes and elongated to take a part of the center, northeast and southwest directions (Fig. 2b). The high and low anomalies are distributed parallel to each other without lots of intersection that helps to give a good explanation of the magnetic distribution bodies under the surface.

Reduction to the magnetic north pole

The total aeromagnetic intensity map is enhanced using the RTP technique. This technique is used to: (1) eliminate the effect of magnetic field inclination and declination, (2) refine the position of magnetic anomalies in respect to the north pole, these anomalies are observed from the north pole, or even reduce the distortion of the magnetic anomaly, and (3) minimize the polarity effects too (Blakely 1996). Depending on Fast Fourier Transform (FFT), the RTP map is derivative from the TMI map by shifting the data to the north pole. This transform makes the magnetic anomalies became overlay the causative magnetic bodies and the anomalies became more accurate and charming in its shape (Fig. 2c).

Analysis of power spectrum transformation

The RTP map is enhanced using high and low band pass filters that is applied using Geosoft program (Oasis Montaj 2015). This technique is applied to make a separation between regional and residual anomalies which may be represented on the analog curve of power spectrum with radial average. Depending on the fast Fourier transform (FFT), the grid is periodically processed on its edge (Lee 1960). By observation and illustration, the power spectrum curve of the study area it is manifested that the deep-seated magnetic component wavenumber varies from 0 to 0.18 cycles/km while the near-surface magnetic component ranges from 0.18 to 0.25 cycles/km. It reveals that there are two main average levels (interfaces) which are intercepted by 0.15 cutoff point. The valid interpretation of the spectrum curve reflects that the regional anomalies of the study area reach about 5680 m while the residual anomalies reach about 2046 m. The power spectrum curve is dissected to three regions with different slopes. The *first* portion represents seated regional magnetic component, the *second* portion represents seated residual magnetic component, and the *last* portion represents white noise that may be reflects the surface features.

The regional-residual separation filter is used to detect and delineate the depth of shallow and deep anomaly (Fig. 3a). The deep anomalies are represented by strong and long wavelength, while the shallow anomalies are represented by weak and short wavelength on the power spectrum curve (Spector and Parker 1979). Depending on the slopes and cutoff points, the regional anomalies are separated from the residual anomalies, where the regional anomalies slope is smaller than the residual anomalies. The depths of the regional and residual anomalies are determined by the following equation (Spector and Grant 1970):

$$h = \frac{-s}{4\pi}, \tag{1}$$

where, h is the depth to the anomalies and s is the slope of magnetic anomalies illustrated on the power spectrum curve.

The regional map is displayed using low pass filter (frequencies are lower than the cutoff point) (Allen and Mills 2004) while the residual map is displayed using high pass filter (frequencies are higher than the cutoff point) (Fig. 3b, c) (Allen and Mills 2004). Inspection of regional magnetic data, it is observed that the regional map represents only high amplitude anomalies more than it appears in RTP map. The regional anomalies are distributed over the study area and are described as following: high anomalies took large places from northern, western, and north-northwestern, and there are also two small anomalies located in ENE and SSE directions. Inspection of residual magnetic data, it is observed that the residual data are represented only low amplitude anomaly ranges that appeared on RTP map. The residual anomalies are distributed over study area with contrast between high anomaly and low anomaly that reflect the appearance of faults in the study area. Fundamentally, residual values reflect the shallow seated magnetic anomaly of the study area.

Edge detecting methods of aeromagnetic data

Vertical derivative

The RTP map is processed using the vertical derivative (VDR) technique which is described as a physical equivalent to detecting magnetic field of two points that locate vertically to each other. This technique is applied by subtracting the magnetic data and dividing the display by the vertical spatial separation of the two points. The result of this technique is represented in frequency equation which leads to enhance the high frequencies corresponding to low frequencies (Fig. 4a). Basically, the derivative technique depends on
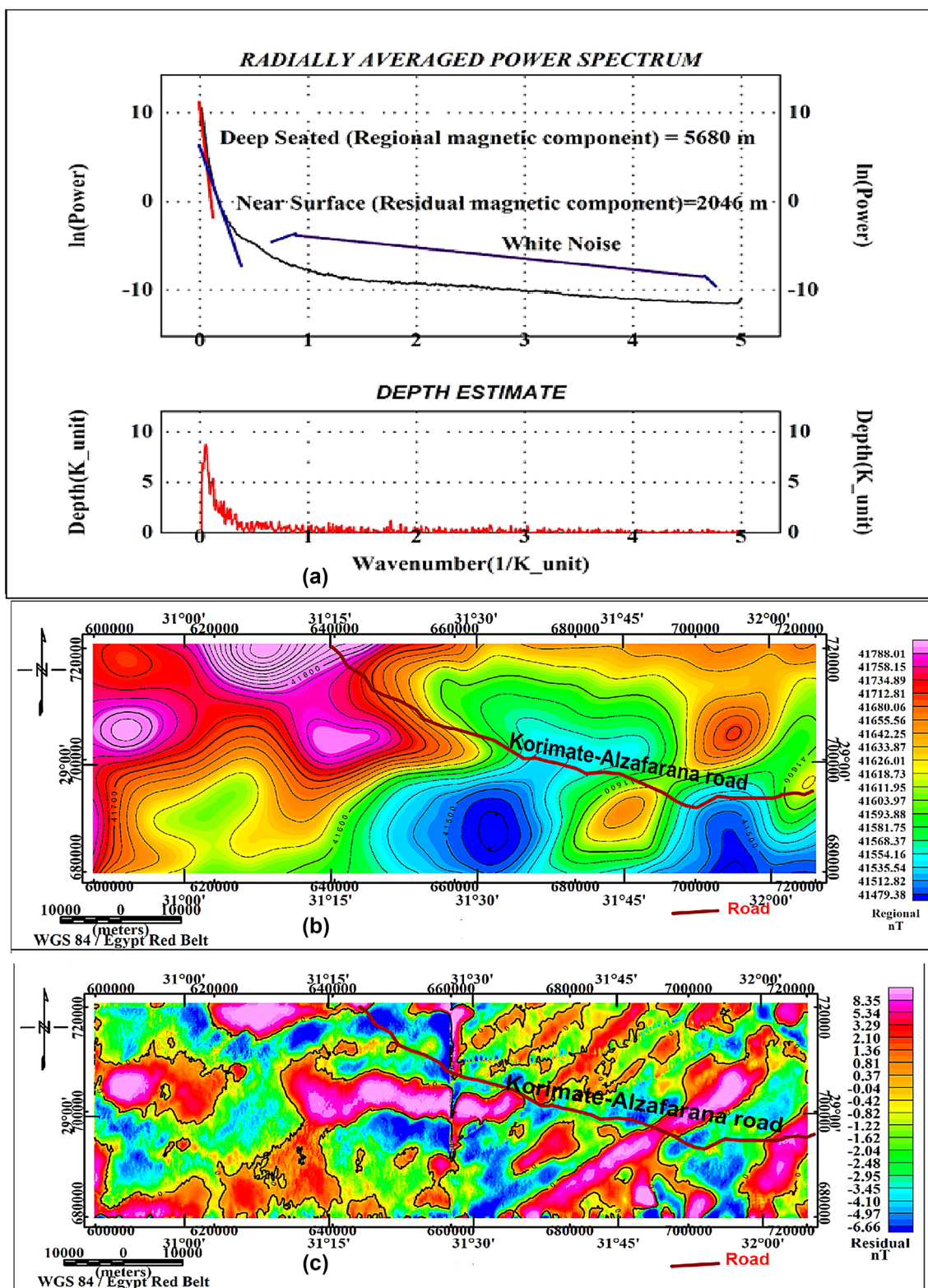
Fig. 3 **a** Radially averaged power spectrum and depth estimation of aeromagnetic sources at the study area. **b** Regional (low-pass filtered) aeromagnetic component of the RTP. **c** Residual (high-pass filtered) aeromagnetic component of the RTP the study area
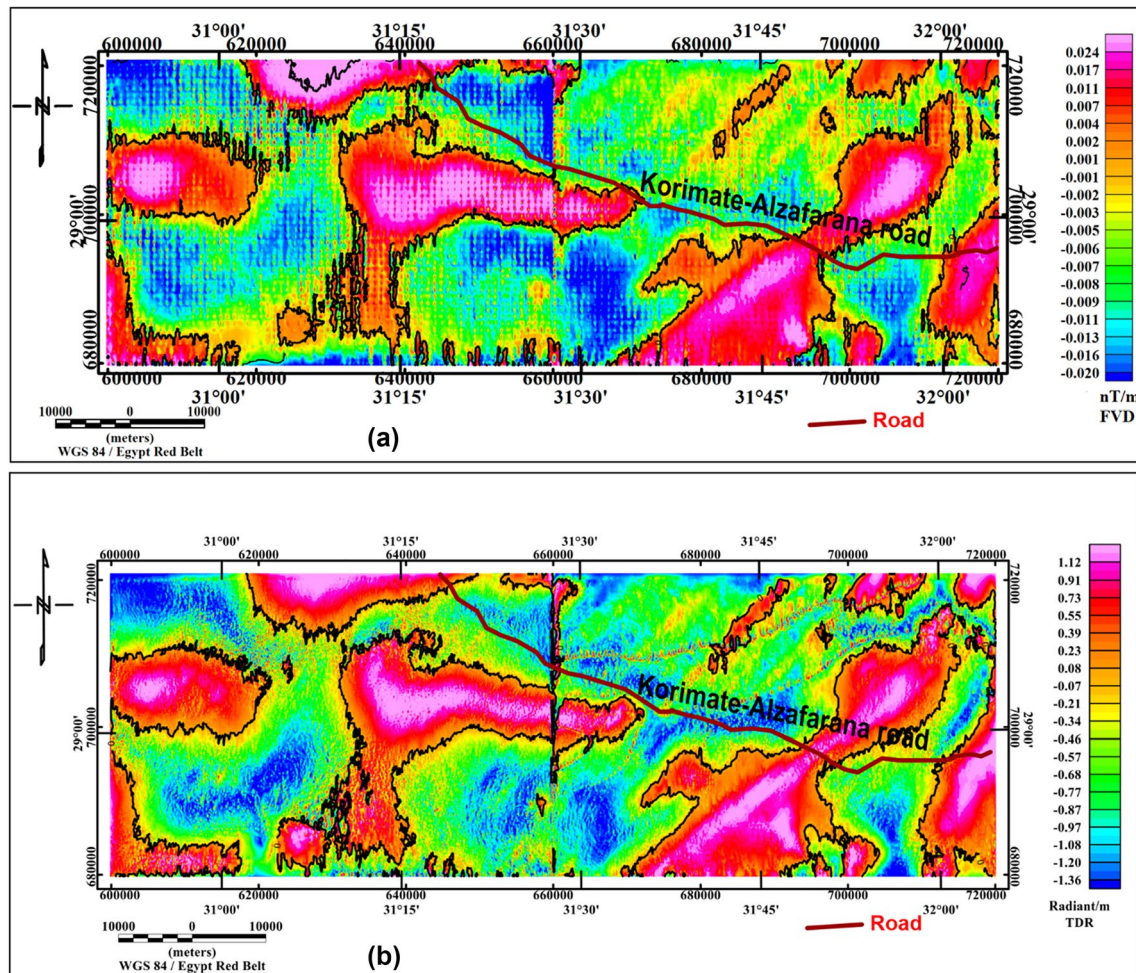
Fig. 4 **a** First vertical derivative map of aeromagnetic data at the study area. **b** Tilt derivative map of aeromagnetic data. The black lines illustrate the zero-radian contour of the tilt angle of the study area

the reduction of the long wavelength-regional effects and determine the properties of adjacent anomalies (Milligan and Gunn 1997). Using first vertical technique, it is easy to delineate the high wave anomalies number that reflects surface, near surface and local geological structures such as (ground water channel).

Tilt derivative

The RTP map is processed using the Tilt Derivative Technique (TDR) (Fig. 4b). Several researchers described the process of the TDR such as: Miller and Singh (1994), Verduzco et al. (2004a, b), Salem et al. (2007), Salem et al. (2008), Fairhead et al. (2008), Hinze et al. (2013). The TDR technique assists to delineate the basement structures

in shallow depths and mineral exploration goals using Geosoft program (Oasis Montaj 2015). The TDR is represented as a tilt angle filter and then is developed to be TDR filter.

The TDR technique represented the sources edge as a zero value which TDR values ranged between $-90°$ to $+90°$ according to VDR while equal to absolute value according to total horizontal derivative (Salem et al. 2008). Using TDR technique, it is very easy to highlight the shallow subsurface structures according to delineate the separation contact between high and low magnetic anomalies that are bordered by contour line with zero value. It is observed that TDR distribution shapes are like first vertical derivative distribution shapes in which there were sudden changes in the values of magnetic anomalies that highlighted the subsurface faults, contacts, and edge
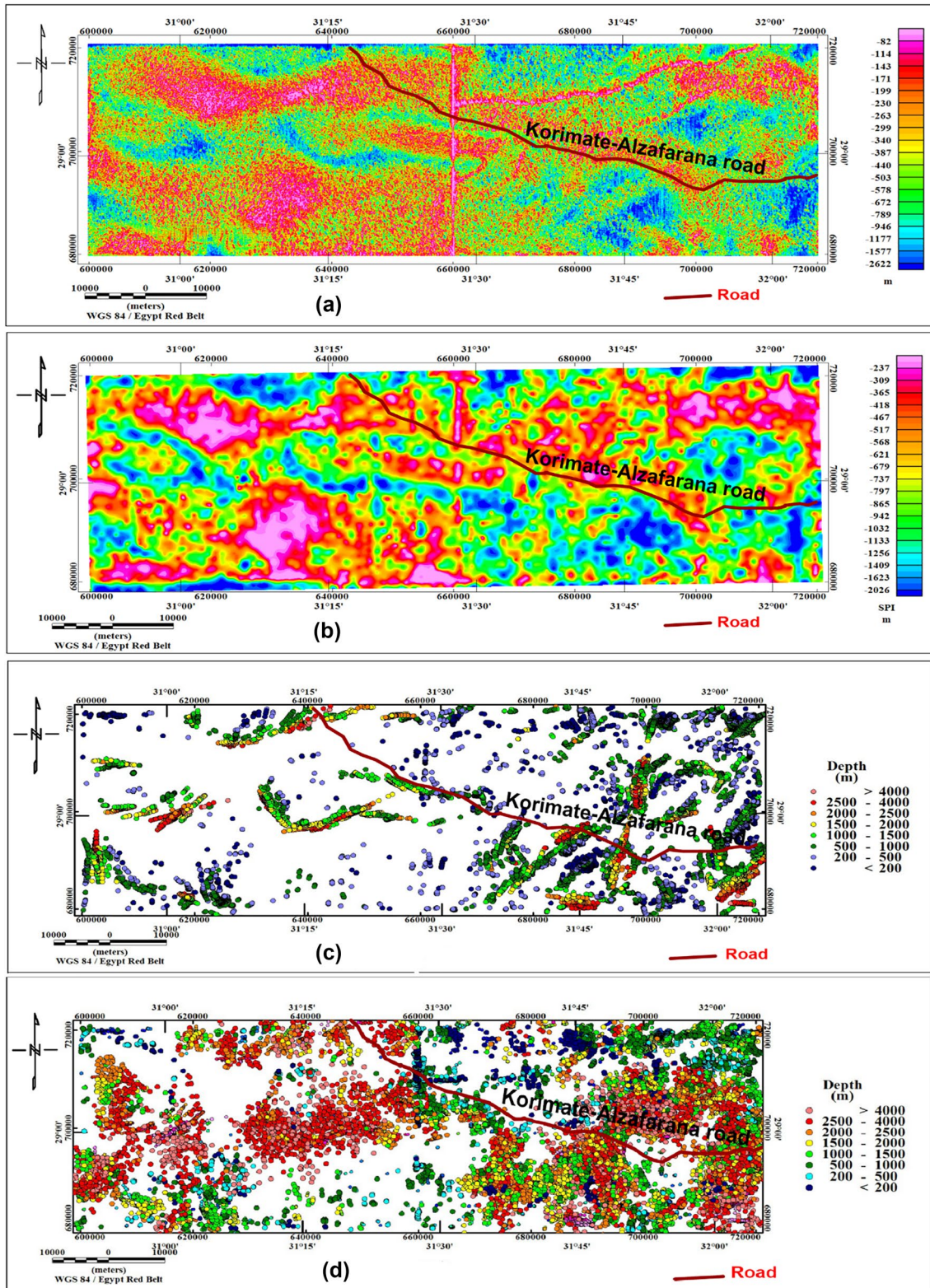
Fig. 5 **a** Depth to magnetic basement as calculated using the AS technique in the study area. **b** Depth to magnetic basement as calculated using the Source parameter imaging technique in the study area. **c** Euler deconvolution method solution using structural index SI = 0. **d** Structural index SI = 1 of the study area

of magnetic sources. The TDR magnetic anomalies have NE–SW, E–W and N–S directions.

Magnetic depth estimation

There are multiple techniques that assist to identify the depth of the basement and the subsurface magnetic bodies such as analytical signal (AS) (Salem et al. 2002), source parameter imaging (SPI) (Thurston and Smith 1997; Thurston et al. 2002; Smith et al. 2005; Smith and Salem 2005), 2D magnetic modeling (Ruotoistenmaki 1993), and Euler deconvolution (ED) (Thompson 1982; Reid et al. 1990; FitzGerald et al. 2004).

Analytical signal (AS) technique

The RTP map is processed in frequency domain using Fast Fourier Transform (FFT) to display the AS map of the study area (Fig. 5a) (Blakely 1995)**.** The AS technique is known as a total gradient which is defined as the square root of summation of VDR of intensity's total magnetic field in the *x*, *y*, and *z* directions (Nabighian 1972; Roest et al. 1992; Macleod et al. 1993). The basic of 3D analytical signal is mainly depicted by Roest et al. (1992) and MacLeod et al. (1993), while the basic of 2D analytical signal is mainly depicted by Green and Stanley (1975), Nabighian (1974).

The 2D case is used for an extremely thin dike and noticeably vertical step or contact, the locations of 2D maximum AS are nonstop above the top surface edges of causative magnetic body (Lin-Ping and Zhi-Ning 1998). In 3D, the AS amplitude depends on; (1) the burial depth, (2) the extent and dipping angle of a source body, (3) the body's magnetization direction, and (4) the direction of earth's magnetic field. In 2D magnetic sources, the analytic signal AS becomes independent on the magnetization direction (Li 2006; Salem et al. 2002). To estimate the magnetic depth by interpreting AS magnetic anomalies, these anomalies reflect the depth of the study area that range between −82 to −2622 m. (Fig. 5a).

Source parameter imaging (SPI) technique

The SPI technique is known as the local wavenumber technique which can be used for the calculaton of the depth to the magnetic bodies. The SPI method is applied using the second order derivatives of the field (Thurston and Smith 1997). Basically, the SPI technique depends on the complex extension AS to estimate the magnetic bodies' depth. The SPI technique is very satisfied on a two-dimension sloping contact or a two-dimension dipping thin sheet (Adham Basheer 2016; Megahed et al. 2020). The SPI map interpretation reflects that the depth of the study area ranged between −237 and −2026 m. (Fig. 5b).

Euler deconvolution (ED) technique

The RTP map is processed using the ED technique on Oasis Montaj, (Geosoft Program 2015) which is used to calculate the depth and location of the potential field sources. The concept of the ED technique was discussed by Reid et al. (1990), Zhang et al. (2000) and Thompson (1982). The ED technique is used to interpret the profile data and after that it is enhanced and used for gridded data (Reid et al. 1990; Klingele et al. 1991; Marson and Klingele 1993; Harris et al. 1996; Stavrev 1997; Barbosa et al. 1999; Barbosa and Medeiros (2001); Mushayandebvu et al. 2001; Salem and Ravat 2003; Silva and Barbosa 2003; Keating and Pilkington 2004; Mushayandebvu et al. 2004).

The ED is used to integrate both geological and geophysical constraints into collected and grouped depth map to illustrate the contact SI. The amplitude function of ED is always positive and independent on the direction of body magnetization (Jeng et al. 2003). Chiefly, the ED depends on the SI which is related positively to the shape of the contributory source. Depending on the least square inversion of the data within a chosen window length, the locations of optimum sources are founded. In the ED maps, the clustering of circles in linear shapes reflects the elongation and the trending of the faults which are taken in N–S, NNE–SSW, NEE–SWW, E–W and NE–SW directions.

The variations in SI values assists to identify different magnetic bodies. The SI value that equals to unity represents the magnetic contact between sedimentary rocks and basement rocks and its depths in study area (Fig. 5c), while the SI value that equal to zero represents the depths of faults in study area (Fig. 5d).

2D magnetic modeling

The best method to appropriate geophysical parameter to potential data is identified as a 2D magnetic modeling. The potential problem is enhanced to be displayed in a potential model which is considered as an inverse solution to potential problem. Depending on the variation in rock properties, the direct modeling process converts the variation in the potential data to a subsurface geological model. To be more satisfied by the geological model, much information about
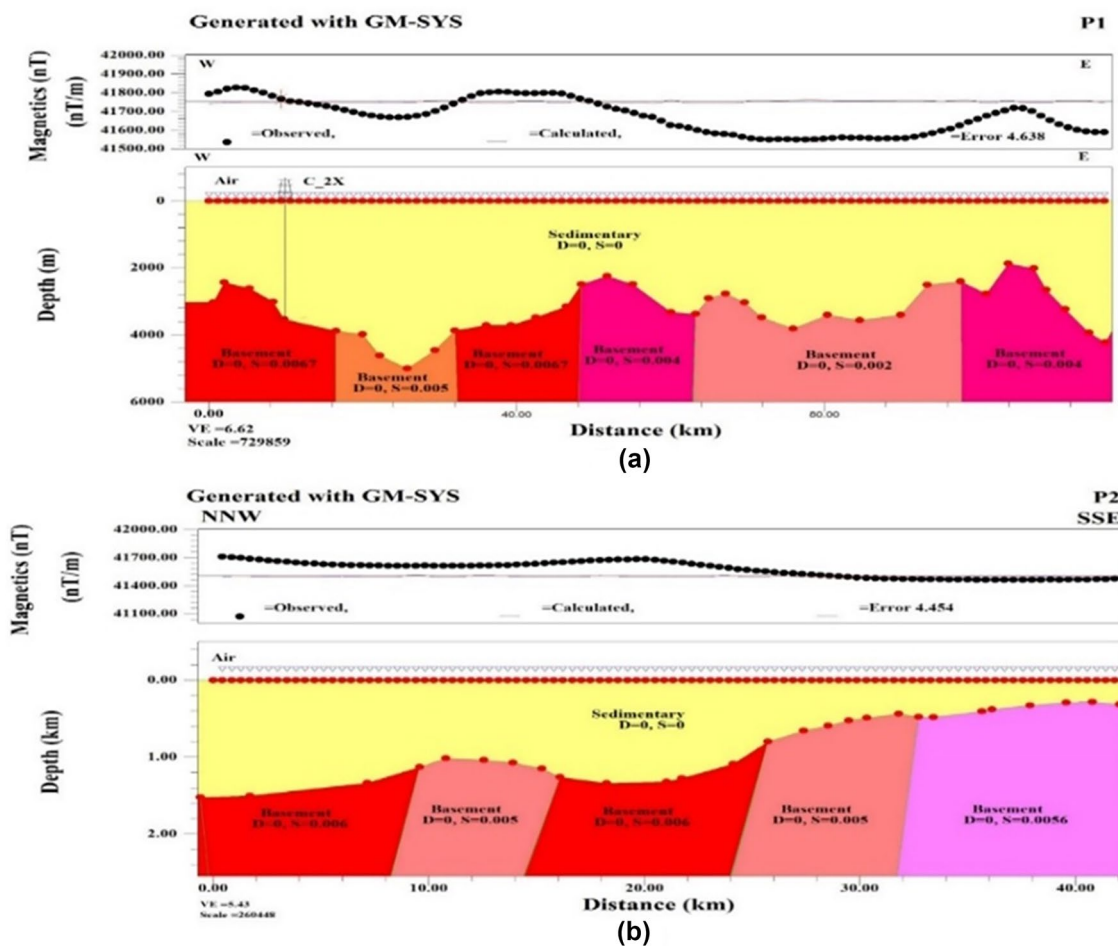
Fig. 6 **a** Two-dimensional magnetic profile (P1) in W–E direction. **b** Two-dimensional magnetic profile (P2) in NNW–SSE direction along the study area

the surface and subsurface magnetic susceptibilities has been collected. The 2D magnetic modeling reflects a good illustration to location, depth, dip, and magnetic susceptibility to the magnetic bodies. Two 2D magnetic profiles (Fig. 6a, b) are constructed by GM-SYS program along the extended magnetic anomaly of RTP map passing from west to east and from NNW to SSE directions (Fig. 2c). These profiles are interpreted basically, depending on the previously geologic information, magnetic depth determination and qualitative interpretation of magnetic maps, to determine the basement depth of the study area. The magnetic susceptibilities range between 0.001 and 0.009 in CGS unit. It assumes to be zero for the nonmagnetic sedimentary cover. Two-dimensional

Table 1 The information of profiles (length and direction)

Profile	Length (m)	Direction
P1	119,335.483	W–E
P2	42,264.8777	NNW–SSE

magnetic modeling technique is formed from observed and calculated magnetic data. These magnetic data are represented by black circle profile while calculated magnetic data are represented by solid black profile (Fig. 6). A best fitting between observed and calculated data is applied depending on the variations in magnetic susceptibilities. The error in fitting is represented in a red line (Fig. 6). The 2D magnetic profile is plotted between *Y* axis that represented depth in meter and *X* axis that represents the horizontal surface distance in kilometer unit (Table 1).

The first 2D profile is taken along RTP map from west to east in the study area. This profile passes through C_2X drilled well that reached the basement with depth 3506.40 m. The total length of this 2D profile is 119,335.483 m from the starting point at the west direction. A good fitting to the observed and calculated data was applied to represent the basement depth with a total error 4.638. This 2D model consists of two parts; *first part* represents the sedimentary cover with magnetic susceptibility equal to zero c.g.s-e.m.u and *second part* represents the susceptibility of basement
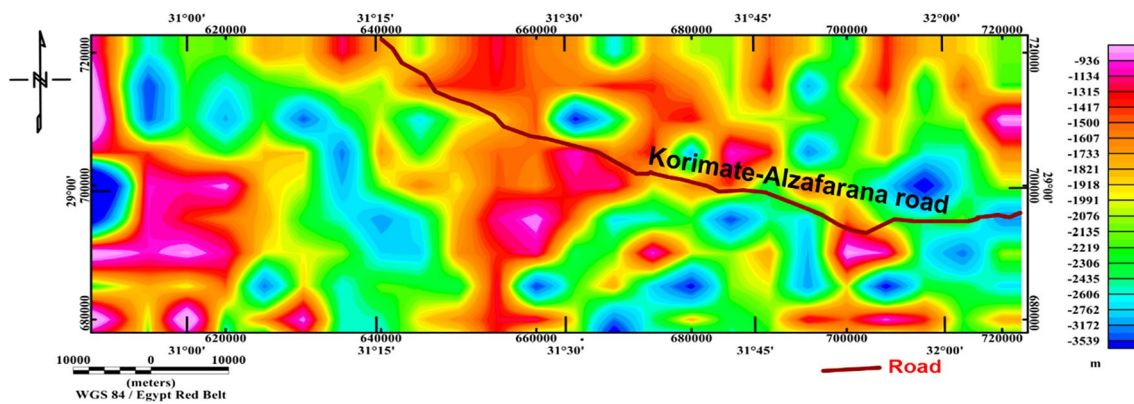
Fig. 7 Basement depth map calculated by the P-depth technique at the study area

rocks which ranged between 0.002 and 0.0067 c.g.s-e.m.u. The total depth of the basement in this profile was ranged between 2000 and 5000 m. The second 2D profile is taken along the RTP map from NNW to SSE in the study area. The total length of this profile is 42,264.8777 m from the starting point at the north direction. A good fitting to the observed and calculated data was applied to represent the basement depth with a total error 4.454. This model consists also of two parts; *first part* represented the sedimentary cover with magnetic susceptibility equal to zero c.g.s-e.m.u and *second part* represented the susceptibility of basement rocks which rocks which ranged between 0.005 and 0.006 c.g.s-e.m.u. The total depth of the basement in this profile was ranged between 1500 and 2000 m.

Finally, by notice, the P-depth map it is observed that the depth to basement of study area ranges between −936 to −3539 m according to seal level. The shallow depths are distributed in western, east-northeastern, southeastern, and the center, while the deep depths range between −936 to −1991 m according to seal level. They elongate from south to north and distribute in many directions within the investigated area (Fig. 7).

Trend analysis technique

Trend analysis technique is considered as a good explanation for the SI and interpretation of geological and geophysical studies. The structural geological interpretation of the study area is magnified using RTP, Residual and 3D ED maps. There is a relationship between the strength of the magnetic anomalies and the crust forces which the tectonic history is represented as a magnetic anomaly (Affleck 1963). Depending on the appearance and existing of magnetic anomalies,

it was easy to delineate the appearance of the faults (Hall 1964). By integrating the results, which obtained from RTP, 3D ED and Residual maps, a good lineament map is displayed to reach the prevailing tectonic pattern in study area (Fig. 8a). Each map detected lineaments with different azimuth and length which may represented faults or contacts. Depending on the azimuth and length of these lineaments, statistical analysis was applied to display structural elemental rose diagram of these maps (Fig. 8b). A good examination of the rose diagram reflects that NE–SW trend is the predominant structural trend affecting on the study area as deducing from magnetic anomalies. Furthermore, there are minor structural trends which are taken N–S, NW–SE, W–E, NNW–SSE and NNE–SSW directions.

Conclusion

The collected aeromagnetic data are used to delineate the subsurface structures at the western part of Koraimat-Alzafarana road and surrounding area in Egypt. By integrated results that are obtained from RTP, 3D Euler deconvolution and residual maps, a satisfied lineament map has been displayed to reach the prevailing tectonic patterns in the area under investigation. Depending on the azimuth and length of these lineaments, statistical analyses are applied to display the structural elemental rose diagram of these maps. A valid examination of rose diagram reflected that the NE–SW trend is the predominant structural trend affecting on the study area as deducing from magnetic anomalies. Moreover, there are minor structural trends which were taken N–S, NW–SE, W–E, NNW–SSE and NNE–SSW directions.
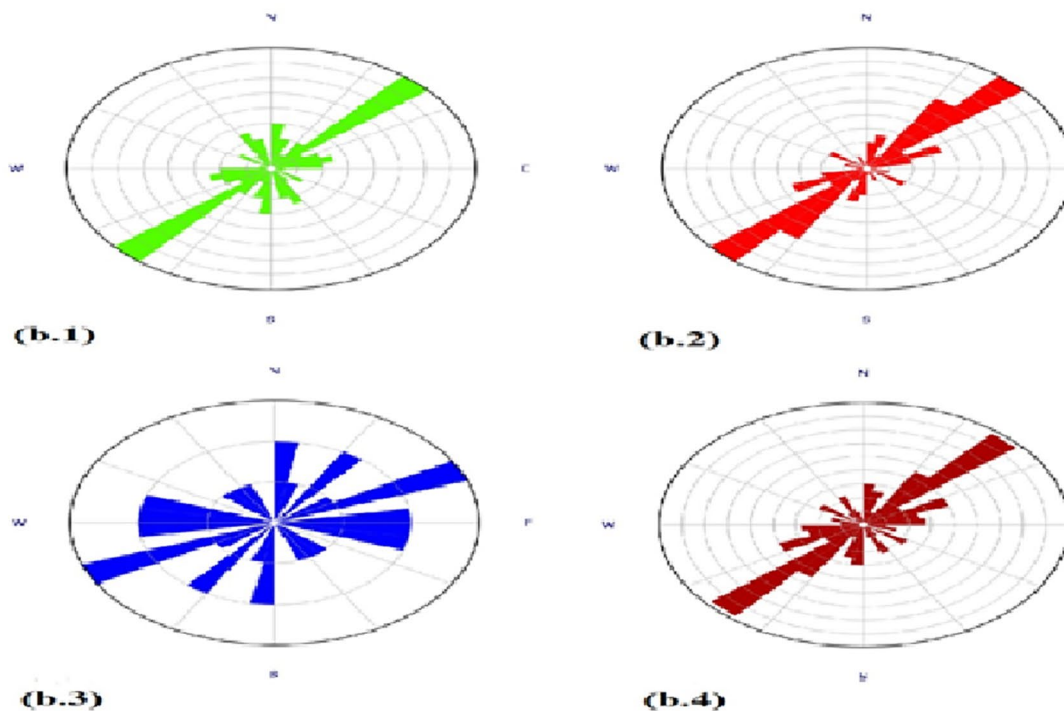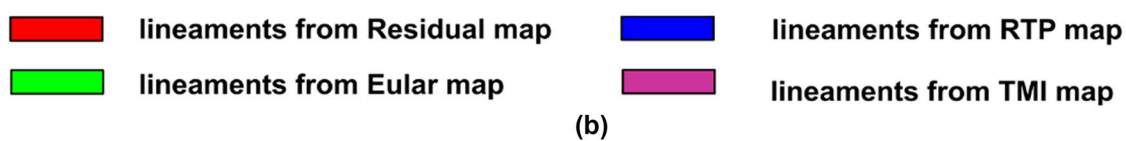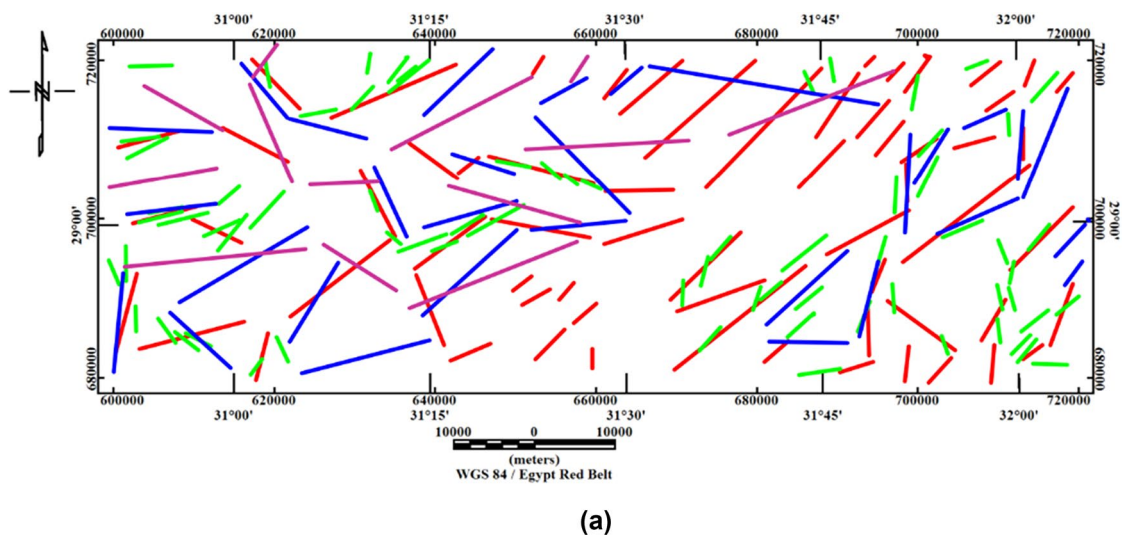
(a)

(b)

(b.1)

(b.2)

(b.3)

(b.4)

Fig. 8 **a** A combined aeromagnetic lineament map of the study area. **b** Rose diagram showing the subsurface structural lineaments that deduced from (b.1) 3D Euler deconvolution analysis map at SI = 0, (b.2) residual anomaly map, (b.3) RTP map and (b.4) total collected lineaments from 3D Euler, residual and RTP maps

References

Alhussein Adham Basheer (2016). Implementation of aeromagnetic data analysis at Wadi Zeidun Area, Central Eastern Desert, Egypt. Int J Geol Earth Sci 2(4). http://www.ijges.com. http://new.ijges. com/uploadfile/2020/0303/20200303104613276.pdf (**ISSN 2395-647X**)

Aero Service (1984). Final operational report of airborne magnetic/radiometric survey in the Eastern Desert, Egypt for the Egyptian General Petroleum Corporation: Aero Service, Houston, Texas, April, six volumes

Affleck J (1963) Magnetic anomaly trend and spacing patterns. Geophysics 28(3):379–395

Alasi TK, Ugwu GZ, Ugwu CM (2017) Estimation of sedimentary thickness using spectral analysis of aeromagnetic data over Abakaliki and Ugep areas of the Lower Benue Trough, Nigeria. Int J Phys Sci 12(21):270–279

Allen RL, Mills D (2004) Signal analysis: time, frequency, scale, and structure. Wiley

Barbosa VCF, Medeiros WE (2001) Scattering, symmetry, and bias analysis of source-position estimates in Euler deconvolution and its practical implications. Geophysics 66(4):1149–1156

Barbosa VC, Silva JB, Medeiros WE (1999) Stability analysis and improvement of structural index estimation in Euler deconvolution. Geophysics 64(1):48–60

Blakely RJ (1995) Potential theory in gravity and magnetic applications. Cambridge University Press

Blakely RJ (1996) Potential theory in gravity and magnetic applications. Cambridge University Press, p 447

CONOCO (1987) Geological map of Egypt, NF 36 NW El Sad El Ali. Scale 1:500000. The Egyptian General Petroleum Corporation GPC and Conoco Co.

Didger (2008) Golden Software; Golden, CO, digitizing software program, Version 3, Shareware software in the category Education developed by Golden Software, Inc.

EROS, U USGS EROS archive—digital elevation—Shuttle Radar Topography Mission (SRTM) 1 Arc-Second Global

Exploration Geophysics (2020) Wikipedia the free encyclopedia. https://en.wikipedia.org/wiki/Exploration_geophysics

Fairhead JD, Salem A, Williams S, Samson E (2008) Magnetic interpretation made easy: the tilt-depth-dip-Δk method. In: SEG technical program expanded abstracts 2008. Society of Exploration Geophysicists, pp 779–783

FitzGerald D, Reid A, McInerney P (2004) New discrimination techniques for Euler deconvolution. Comput Geosci 30:461–469

G Program (Oasis Montaj) (2015) Aero Service Company, Mineral Petroleum Ground- Water Assessment Program (MAGMAP), 2-D frequency-domain processing. Geosoft Inc., Toronto

Geosyntec (2004) Toolkit topics. Connecticut Department of Environmental Conservation Connecticut Stormwater Quality Manual. https://megamanual.geosyntec.com/npsmanual/subsurfacerechargestructures.aspx

Green R, Stanley JM (1975) Application of a Hilbert transform method to the interpretation of surface-vehicle magnetic data. Geophys Prospect 23(1):18–27

Hall DH (1964) Magnetic and tectonic regionalization on Texada Island. BC Geophys 29(4):565–581

Harris E, Jessell M, Barr T (1996) Analysis of the Euler deconvolution technique for calculating regional depth to basement in an area of complex structure. In: SEG Technical Program Expanded Abstracts 1996. Society of Exploration Geophysicists

Hinze WJ, Von Frese RR, Von Frese R, Saad AH (2013) Gravity and magnetic exploration: principles, practices, and applications. Cambridge University Press

Jeng Y, Lee YL, Chen CY, Lin MJ (2003) Integrated signal enhancements in magnetic investigation in archaeology. J Appl Geophys 53(1):31–48

Joshua EO, Layade GO, Adewuyi SO (2018) Analytic signal method (Hilbert solution) for the investigation of iron-ore deposit using aeromagnetic data of Akunnu-Akoko Area, Southwest, Nigeria. Phys Sci Int J 17:1–9

Keating P, Pilkington M (2004) Euler deconvolution of the analytic signal and its application to magnetic interpretation. Geophys Prospect 52(3):165–182

Khalil A, Abdel Hafeez TH, Saleh HS, Mohamed WH (2016) Inferring the subsurface basement depth and the structural trends as deduced from aeromagnetic data at West Beni Suef area, Western Desert, Egypt. NRIAG J Astron Geophys 5(2):380–392

Klingele EE, Marson I, Kahle HG (1991) Automatic interpretation of gravity gradiometric data in two dimensions: vertical gradient 1. Geophys Prospect 39(3):407–434

Lee YW (1960) Statistical theory of communication. Am J Phys 29(4):276–278 (**pp 1–75**)

Li X (2006) Understanding 3D analytic signal amplitude. Geophysics 71(2):L13–L16

Lin-Ping H, Zhi-Ning G (1998) On: "Magnetic interpretation using the 3-D analytic signal" (Walter R. Roest, Jacob Verhoef, and Mark Pilkington, GEOPHYSICS, 57, 116–125). Geophysics 63(2):667–670

Lisle RJ (2006) Google Earth: a new geological resource. Geol Today 22(1):29–32

MacLeod IN, Jones K, Dai TF (1993) 3-D analytic signal in the interpretation of total magnetic field data at low magnetic latitudes. Explor Geophys 24(4):679–688

Marson I, Klingele EE (1993) Advantages of using the vertical gradient of gravity for 3-D interpretation. Geophysics 58(11):349–355

Megahed AA, Omran MA, Selim EI, Basheer AA (2020) Implementation of magnetic technique to delineate the subsurface tectonic trends of Wadi Barqa surrounding area, southeast of Sinai Peninsula, Egypt. IOSR J Appl Geol Geophys (IOSR-JAGG) 8(5 Ser. I):15–23. https://webcache.googleusercontent.com/search?q=cache:UrEHNKVKfz0J:https://www.iosrjournals.org/iosr-jagg/papers/Vol.%25208%2520Issue%25205/Series-1/B0805011523.pdf+&cd=1&hl=ar&ct=clnk&gl=eg

MHUUD (2015) Environmental characterization of the new city of Beni Suef. https://www.eeaa.gov.eg/portals/0/eeaaReports/NewCitiesProfile/banisuef.pdf

Miller HG, Singh V (1994) Potential field tilt—a new concept for location of potential field sources. J Appl Geophys 32(2–3):213–217

Milligan PR, Gunn PJ (1997) Enhancement and presentation of airborne geophysical data. J Aust Geol Geophys 17(2):63–75

Mosaad S, Kehew AE (2019) Integration of geochemical data to assess the groundwater quality in a carbonate aquifer in the southeast of Beni-Suef city. Egypt. J Afr Earth Sci 158:103558

Mushayandebvu MF, van Driel P, Reid AB, Fairhead JD (2001) Magnetic source parameters of two-dimensional structures using extended Euler deconvolution. Geophysics 66(3):814–823

Mushayandebvu MF, Lesur V, Reid AB, Fairhead JD (2004) Grid Euler deconvolution with constraints for 2D structures. Geophysics 69(2):489–496

Nabighian MN (1972) The analytic signal of two-dimensional magnetic bodies with polygonal cross-section: its properties and use for automated anomaly interpretation. Geophysics 37(3):507–517

Nabighian MN (1974) Additional comments on the analytic signal of two-dimensional magnetic bodies with polygonal cross-section. Geophysics 39(1):85–92

Nwankwo LI (2014) Discussion on spectral analysis of aeromagnetic data for geothermal energy investigation of Ikogosi Warm Spring—Ekiti State, southwestern Nigeria. Geotherm Energy 2:11. https://doi.org/10.1186/s40517-014-0011-3

Reeves C (2005) Aeromagnetic surveys: principles, practice and interpretation, vol 155. Geosoft, Washington (DC)

Reford MS (1962) Magnetic anomalies over thin sheets. Geophysics 29(4):532–536

Reid AB, Allsop JM, Granser H, Millett AT, Somerton IW (1990) Magnetic interpretation in three dimensions using Euler deconvolution. Geophysics 55(1):80–91

Roest WR, Verhoef J, Pilkington M (1992) Magnetic interpretation using the 3-D analytic signal. Geophysics 57(1):116–125

Ruotoistenmaki T (1993) The magnetic anomaly of 3D sources having arbitrary geometry and magnetization. Geophys Prospect 41(4):413–433

Saber SG, Salama YF (2017) Facies analysis and sequence stratigraphy of the Eocene successions, east Beni Suef area, eastern Desert. Egypt J Afr Earth Sci 135:173–185

Said R (1962) The geology of Egypt. Elsevier Publ. Co., Amestrdam

Salem A, Ravat D (2003) A combined analytic signal and Euler method (AN-EUL) for automatic interpretation of magnetic data. Geophysics 68(6):1952–1961

Salem A, Ushijima K, Elsirafi A, Mizunaga H (2000) Spectral analysis of aeromagnetic data for geothermal reconnaissance of Quseir area, northern Red Sea, Egypt. In: Proceedings of the world geothermal congress, vol 16691674

Salem A, Ravat D, Gamey TJ, Ushijima K (2002) Analytic signal approach and its applicability in environmental magnetic investigations. J Appl Geophys 49(4):231–244

Salem A, Williams S, Fairhead JD, Ravat D, Smith R (2007) Tilt-depth method: a simple depth estimation method using first-order magnetic derivatives. Lead Edge 26(12):1502–1505

Salem A, Williams S, Fairhead D, Smith R, Ravat D (2008) Interpretation of magnetic data using tilt-angle derivatives. Geophysics 73(1):L1–L10

Sayed DM, El-Shazly SH, Salama YF, Badawy HS, Abd El-Gaied IM (2021) Macropaleontological and paleobiogeographical study of the Upper Eocene succession at Beni-Suef-Zaafrana road, north Eastern Desert, Egypt. J Afr Earth Sci 174:104046

Silva JB, Barbosa VC (2003) 3D Euler deconvolution: theoretical basis for automatically selecting good solutions. Geophysics 68(6):1962–1968

Smith RS, Salem A (2005) Imaging depth, structure, and susceptibility from magnetic data: the advanced source-parameter imaging method. Geophysics 70(4):L31–L38

Smith RS, Salem A, Lemieux J (2005) An enhanced method for source parameter imaging of magnetic data collected for mineral exploration. Geophys Prospect 53(5):655–665

Sordi DAD (2007) Aerogeofísica aplicada à compreensão do sistema de empurrões da sequência Santa Terezinha de Goiás, Brasil central

Spector A, Grant FS (1970) Statistical models for interpreting aeromagnetic data. Geophysics 35(2):293–302

Spector A, Parker W (1979) Computer compilation and interpretation of geophysical data. In: Hood PJ (ed) Geol. Sur. of Canada, Economic geology Report 31, pp 527–544

Stavrev PY (1997) Euler deconvolution using differential similarity transformations of gravity or magnetic anomalies [Link]. Geophys Prospect 45(2):207–246

Tahoun SS, Deaf AS, Mansour A (2017) Palynological, palaeoenvironmental and sequence stratigraphical analyses of a Turonian-Coniacian sequence, Beni Suef Basin, Eastern Desert, Egypt: implication of pediastrum rhythmic signature. Mar Pet Geol 88:871–887

Thompson DT (1982) EULDPH: a new technique for making computer-assisted depth estimates from magnetic data. Geophysics 47(1):31–37. https://doi.org/10.1190/1.1441278

Thurston JB, Smith RS (1997) Automatic conversion of magnetic data to depth, dip, and susceptibility contrast using the SPI (TM) method. Geophysics 62(3):807–813

Thurston JB, Smith RS, Guillon JC (2002) Amultimodel method for depth estimation from magnetic data. Geophysics 67(2):555–561

Verduzco B, Fairhead JD, Green CM, MacKenzie C (2004a) New insights into magnetic derivatives for structural mapping. Lead Edge 23(2):89–95

Verduzco B, Fairhead JD, Green CM, MacKenzie C (2004b) New insights into magnetic derivatives for structural mapping. Lead Edge 23(2):116–119

Waheed HM (2019) Geophysical studies for hydrocarbon reservoir exploration at west Beni Suef Area, Western Desert, Egypt. Al-Azhar University, Faculty of Science, Geology Department, M.Sc. Master's Degree

Zahran H, Elyazid KA, Mohamad M (2011) Beni Suef Basin the key for exploration future success in Upper Egypt. Search and Discovery Article, 10351

Zhang C, Mushayandebvu MF, Reid AB, Fairhead JD, Odegard ME (2000) Euler deconvolution of gravity tensor gradient data. Geophysics 65(2):512–520